

Explosion Energies for Core-collapse Supernovae I: Analytic, Spherically Symmetric Solutions

Mariam Gogilashvili,¹ [★] Jeremiah W. Murphy,¹ [†] Quintin Mabanta¹

¹*Department of Physics, Florida State University, 77 Chieftan Way, Tallahassee, FL 32306, USA*

30 April 2022

ABSTRACT

Recent multi-dimensional simulations of core-collapse supernovae are producing successful explosions and explosion-energy predictions. In general, the explosion-energy evolution is monotonic and relatively smooth, suggesting a possible analytic solution. We derive analytic solutions for the expansion of the gain region under the following assumptions: spherical symmetry, one-zone shell, and powered by neutrinos and α particle recombination. We consider two hypotheses: I) explosion energy is powered by neutrinos and α recombination, II) explosion energy is powered by neutrinos alone. Under these assumptions, we derive the fundamental dimensionless parameters and analytic scalings. For the neutrino-only hypothesis (II), the asymptotic explosion energy scales as $E_\infty \approx 1.5M_g v_0^2 \eta^{2/3}$, where M_g is the gain mass, v_0 is the free-fall velocity at the shock, and η is a ratio of the heating and dynamical time scales. Including both neutrinos and recombination (hypothesis I), the asymptotic explosion energy is $E_\infty \approx M_g v_0^2 (1.5\eta^{2/3} + \beta f(\rho_0))$, where β is the dimensionless recombination parameter. We use Bayesian inference to fit these analytic models to simulations. Both hypotheses fit the simulations of the lowest progenitor masses that tend to explode spherically. The fits do not prefer hypothesis I or II; however, prior investigations suggest that α recombination is important. As expected, neither hypothesis fits the higher-mass simulations that exhibit aspherical explosions. In summary, this explosion-energy theory is consistent with the spherical explosions of low progenitor masses; the inconsistency with higher progenitor-mass simulations suggests that a theory for them must include aspherical dynamics.

Key words: Supernovae: general — hydrodynamics — methods: analytical — methods: numerical — methods: statistical

1 INTRODUCTION

The final fate for most massive stars is a core-collapse supernova (CCSN). As one of the most energetic transients in the Universe, CCSNe are important for a wide range of astrophysical origins and processes. If the explosion succeeds, then they leave behind a neutron star; if it fails, then the star collapses to a black hole. CCSNe are major contributors to nucleosynthesis (Woosley et al. 2002). The kinetic energy released is a major contributor to turbulence in the ISM, and is likely a major component of stellar evolution feedback (Mac Low & Klessen 2004). Their importance have inspired theorists and simulators for decades, and recent advancements in multi-dimensional simulations are leading to successful explosions and explosion energy evolution curves. In this manuscript, we develop an analytic theory to explain

the explosion energy evolution of these multi-dimensional simulations.

The fundamental challenges of core-collapse supernova theory are to explain how collapse reverses into explosion, predict which stars will explode, and to predict explosion energies, neutron star masses, etc. Just before explosion, the Fe core collapses, bounces at nuclear densities, and launches a shock wave that then stalls into an accretion shock. The shock stalls due to a combination of Fe disassociation at the shock, neutrino losses, and the ram pressure of the collapsing star. If the star is to explode, a significant fraction of the binding energy of the protoneutron star must be transported out to the region just behind the shock. Colgate & White (1966) and Bethe & Wilson (1985) showed that neutrinos are instrumental in transporting thermal energy from the protoneutron star to the postshock region; this neutrino transport of energy may then relaunch the stalled shock into an explosion. However, several decades of one-dimensional neutrino transport and hydrodynamic simula-

[★] Email: mg18u@my.fsu.edu

[†] Email: jwmurphy@fsu.edu

tions show that this delayed neutrino mechanism works in spherically symmetric simulations in only the lowest mass progenitors (Liebendörfer et al. 2001a,b, 2005; Rampp & Janka 2002; Buras et al. 2003, 2006; Thompson et al. 2003; Kitaura et al. 2006; Müller et al. 2017; Radice et al. 2017).

Multi-dimensional simulations succeed in exploding where one-dimensional simulations fail (Benz et al. 1994; Herant et al. 1994; Burrows et al. 1995; Janka & Mueller 1995). Murphy & Burrows (2008) showed that the critical condition for explosion is 30% lower in multi-dimensional simulations, and Mabanta & Murphy (2018) showed that neutrino driven convection (and mostly turbulent dissipation) is responsible for this reduction. Multi-dimensional simulations which simulate both multi-dimensional neutrino transport and hydrodynamics are computationally expensive, of order 10 million cpu-hours for three-dimensional simulations. To date, there are only ~ 20 simulations with successful explosions and explosion energy predictions (Lentz et al. 2015; Bruenn et al. 2006, 2016a; Müller 2015; Müller et al. 2019; Vartanyan et al. 2018a; Skinner et al. 2019; Steiner et al. 2013; Vartanyan et al. 2018b).

Simulations are important theoretical tools that provide guidance in the understanding of a complex, nonlinear process. They also promise to provide accurate predictions. On the other hand, their expense do not allow for large systematic studies, and their complexity make it difficult to understand the fundamental physics and conditions for explosion. If possible, analytic investigations are both less computationally expensive and provide a deeper understanding of the theory. In turn, this deeper understanding can help guide further investigations using limited resources available for simulations.

There are now ~ 20 multi-dimensional simulations that successfully explode (Lentz et al. 2015; Bruenn et al. 2006, 2016a; Müller 2015; Müller et al. 2019; Vartanyan et al. 2018a; Skinner et al. 2019; Steiner et al. 2013; Vartanyan et al. 2018b), and the explosion energy curves of these simulations exhibit two characteristics that encourage analytic investigations. For one, the explosion energies are systematically under-energetic compared to explosion energies inferred from observations (Murphy et al. 2019). An analytic investigation may provide a deeper understanding of why they differ. Part of this deeper understanding would include identifying the important dimensionless parameters of the problem. Knowing the important parameters will enable theoretical sensitivity studies. For example, one could identify how much the neutrino luminosity, neutrino cross-section, etc. must increase so that the simulations would match the observations. The second characteristic that encourages analytic investigations is that explosion energy curves show a smooth monotonic increase with time. This suggests that one may develop an analytic or semi-analytic theory describing the explosion energy of CCSNe. Our goal is to derive analytic scalings for the explosion energy evolution, and use these scalings to understand the sensitivity of the explosion energy to the important parameters of the problem.

There have been attempts to derive an analytic expression for explosion energy. Janka (2001) considered the delayed-neutrino mechanism and developed a toy model based on the approximate solution of the hydrodynamic equations. In this model, there are three layers: the cooling layer (bounded by neutrinosphere below and gain region

above), the heating layer (between the gain radius and the shock), and the infall layer (outside the shock). The two lower layers are assumed to be in hydrostatic equilibrium. They solved a boundary value problem at the shock and derived explosion conditions. They found that if the star explodes, then the energy of the gain region can be at most $(2-3) \times 10^{51} \text{ erg}$. However, this study does not infer the important scalings and parameters of the problem.

In another analytic study, Müller et al. (2016) also consider the delayed-neutrino mechanism and derive explosion energies based upon the structure of the progenitor. In this model, the explosion phase is described by simple ODEs that take into account continuous accretion after shock revival. In the pre-explosion phase, they considered a layered model similar to Janka (2001). To simplify the calculations, they use a one-zone approximation in the explosion phase. This model assumes that the explosion energy is mostly due to recombination energy. With these assumptions Müller et al. (2016) derive an ODE and numerically calculate explosion energy for a given stellar structure and composition. This model produces explosions with energies up to $2 \times 10^{51} \text{ erg}$. However, this study did not solve the ODE analytically.

In a third study, Papish et al. (2015) developed an order of magnitude analysis of the explosion energy evolution. They conclude that explosions with delayed-neutrino mechanism cannot give explosion energies $> 0.5 \times 10^{51} \text{ erg}$. However, their explosion energy analysis assumes a steep sensitivity on the gain radius: $E \propto r_{\text{gain}}^{-3}$. Changing the radius of the gain region by a factor of 2 changes the explosion energy by a factor of 10. Given this steep sensitivity on one parameter, it is not obvious that the delayed-neutrino mechanism does not work.

As a final remark, none of these previous studies compared their derivations with multi-dimensional simulations. In this manuscript, one of our primary goals is to test the predictions of the analytic theory that we derive. Specifically, we will use Bayesian fitting techniques to infer values for the theoretical parameters. We will also assess the robustness of fit. In this way, we will either rule out the analytic theories or show that they are consistent with multi-dimensional simulations.

Before further discussing our theory, assumptions, and procedure, we discuss the possible importance of Fe recombination in the explosion energy evolution. Previous investigations suggest that neutrinos and/or Fe recombination are important in determining the explosion energy evolution. One of the primary roles of neutrinos in the explosion is to transport thermal energy from the proto-neutron star outward in radius $\sim 150 \text{ km}$ (Colgate & White 1966; Bethe & Wilson 1985). While the proto-neutron star becomes more bound, there is an opportunity for the gain region and overlying layers to become unbound. Hence neutrinos certainly play some role in the explosion dynamics.

Fe dissociation and recombination may also play an important role in the explosion energy evolution. Before collapse, the core is composed of bound (Fe) nuclei. During collapse, thermal photodissociation unbinds these nuclei into free neutrons, protons, and alpha particles (Fernández & Thompson 2009). This occurs at around a temperature of $T \sim 9 \text{ MeV}$ (the binding energy of Fe is 8.8 MeV per nucleon). This “loss” of energy during collapse causes the collapsing material to have a softer equation of state and be

come more bound. Without this loss of energy or softening of the equation of state, the initial bounce shock might have exploded the star; however, Fe dissociation and neutrino losses ensure that the shock stalls at least momentarily before it revives into explosion. During explosion, the expanding material cools, and the free neutrons, protons, and neutrons recombine to form, first alpha particles and then Fe-group nuclei. This recombination adds thermal energy back into the material.

It is unclear whether Fe recombination has a net effect on the explosion energy evolution. Technically, every instance of Fe recombination (energy injection) started with Fe dissociation (energy loss). In principle, the net effect of Fe dissociation and Fe recombination is zero. However, the transport of energy by neutrinos may complicate this. Müller et al. (2016) noted that for low-energy two-dimensional explosions, the explosion energy was proportional to the total Fe recombination energy. They suggest that explosion is initiated when neutrinos heat the gain region just enough to compensate for initial losses due to Fe dissociation. They then suggest that the explosion energy is set by the mass of the gain region and the Fe recombination energy. However, it is not clear whether this actually happens. For example, Murphy & Dolence (2017) show that the critical condition for explosion is satisfied when the gain region can no longer support hydrostatic equilibrium. If this is connected to the original Fe dissociation, then it is not obvious. Furthermore, it is not clear if the explosion energies of the most recent simulations follow the same correlation between Fe recombination energy and explosion energy.

Since it is not clear whether Fe recombination contributes to the explosion energy, we consider two hypotheses when deriving analytic explosion energy evolution. The first hypothesis (I) is that both neutrino power and Fe recombination contribute to the explosion energy. The second hypothesis (II) is that only neutrino power contributes to net explosion energy because Fe dissociation and Fe recombination cancel.

Inspired by the need for a deeper understanding and the smooth monotonic curves, we use a simple model to derive the explosion energy curve. We develop a one-zone, one-dimensional hydrodynamical model. In this model, the gain region initially is in hydrostatic equilibrium. We also assume that the delayed neutrino mechanism initiates the explosion. We assume that as the explosion begins, the mass accretion rate through the gain region is zero. Since this model is spherically symmetric, we expect our model to successfully describe spherical explosions but fail at describing explosion dominated by aspherical motions. Since lower mass stars mostly explode with spherical symmetry, and higher mass stars mostly explode aspherically, we expect our theory to be consistent with the explosion of lower mass stars and to be inconsistent with higher mass stars. Our final goal is to compare the analytic solutions to simulations.

The structure of this manuscript is as follows. Section 2 presents our theoretical derivation. First, we identify our assumptions and derive the basic dimensionless ODEs. To derive the dimensionless equations, we propose important dimensionless parameters. In addition, we derive analytic scalings, making predictions on how the explosion energy depends upon the dimensionless parameters. In section 3, we compare the analytic theory with existing multi-dimensional

simulations. Using Bayesian analysis, we fit our theory to simulations and determine which are actually good fits. Finally, in section 4, we summarize our results, discuss the physical implications of our theoretical model, and suggest ways in which future simulations may disprove this analytic theory.

2 A SIMPLE THEORY FOR CCSN-EXPLOSION-ENERGY EVOLUTION

To derive analytic scalings for the explosion energy evolution, we develop a one-zone model. In this derivation, we start with the full hydrodynamics equations and are explicit about the assumptions in this one-zone model. This method of approximation ensures that the model is self-consistent and qualitatively includes all relevant physics. While this model will not be quantitatively accurate, it will illuminate important qualitative aspects of the theory. For example, this approach leads to a set of natural dimensionless parameters and scaling relations.

Figure 1 shows a schematic of the one-zone model and illustrates important assumptions of this model. For one, we assume spherical symmetry. Second, we model the dynamic evolution of the gain region. As CCSN simulations begin to explode, the gain region (where neutrino heating dominates neutrino cooling) starts to become unbound and expands (Bethe & Wilson 1985). This gain region begins in near hydrostatic balance and explosion begins when the structure can no longer maintain a hydrostatic structure (Murphy & Dolence 2017). Hence a third major assumption is that the gain region begins in hydrostatic balance. Before explosion, during the stalled phase, the mass accretion through the gain region is nonzero; as the region begins to explode, mass accretion halts and reverses into explosion. To simplify the parameters and equations, the fourth major assumption is that the mass accretion rate is zero through the gain region.

The model also assumes that explosion is driven by neutrinos and/or α recombination. We consider two hypotheses:

- I) Explosion is powered by both neutrinos and α recombination. Müller et al. (2016) suggests that explosion initiates when neutrinos heat the gain region enough to compensate for the losses by Fe dissociation. Thus, neutrinos only contribute to unbind the system. As a result, the system starts to explode from hydrostatic equilibrium and explosion energy is mostly set by Fe recombination. Later, we show that both neutrinos and α recombination can have a comparable impact on the explosion energy.
- II) Explosion is powered by neutrinos alone. When the core collapses at a temperature $T \sim 8.8 \text{ MeV}$, Fe dissociates into nucleons and in doing so, the system becomes more bound by $\sim \epsilon_{\text{rec}} M_g / m_p$. Later, in the explosion phase, nucleons again recombine to bound nuclei, which deposits approximately the same amount of energy $\sim \epsilon_{\text{rec}} M_g / m_p$. If this is true, then Fe recombination has no effect on the explosion energy and only the neutrino power dictates the explosion energy.

Our goal in this manuscript is not to solve the full numerical solution but to derive the important dimensionless parameters and analytic scaling relations that govern the

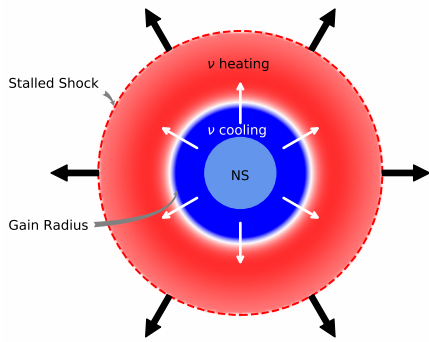


Figure 1. Diagram for the spherical, one-zone explosion model. In this model, $t = 0$ corresponds to the initiation of explosion: when postshock pressure begins to overwhelm gravity (Murphy & Dolence 2017). We model the energy evolution of the gain region in a one-zone approximation. Neutrino heating accelerates material in the gain region outwards and it expands spherically. For initial conditions, the gain region is in hydrostatic balance with a neutrino power source below.

energy evolution for spherically symmetric explosions. To facilitate these analytic derivations, we assume a one-zone spherically symmetric model for the dynamic evolution of the gain region.

2.1 Fundamental Equations and Dimensionless Parameters

The hydrodynamics equations for conservation of mass, momentum, and energy are:

$$\frac{\partial \rho}{\partial t} + \nabla \cdot (\rho \mathbf{v}) = 0, \quad (1)$$

$$\rho \frac{d\mathbf{v}}{dt} = -\nabla p - \rho \nabla \Phi, \quad (2)$$

and

$$\rho \frac{d\epsilon}{dt} = -p \nabla \cdot \mathbf{v} + \rho q_\nu + \rho q_\alpha, \quad (3)$$

ρ is the mass density, \mathbf{v} is the velocity, p is the pressure, ϵ is the specific internal energy, Φ is the gravitational potential, q_ν is the local specific neutrino heating term, q_α is the change in internal energy due to α recombination. To facilitate analytic solutions, we assume a polytropic equation of state (EoS), $P = (\gamma - 1)\rho\epsilon$. For gravity, we assume a simple Newtonian potential, $\Phi = -\frac{GM_{NS}}{r}$, and for neutrino heating, a simple neutrino heating profile of $q_\nu = \frac{L_\nu \kappa}{4\pi r^2}$. The neutrino opacity is $\kappa = \frac{\sigma}{m_p}$.

The difference in hypotheses I and II are the source terms in eq. (3). For hypothesis I, we include both the neutrino and α recombination terms. For hypothesis II, we include only the term related to neutrino heating. Within the gain region, neutrino cooling is much weaker than neutrino heating. Therefore, we neglect neutrino cooling.

To construct the dynamic equations for the spherical

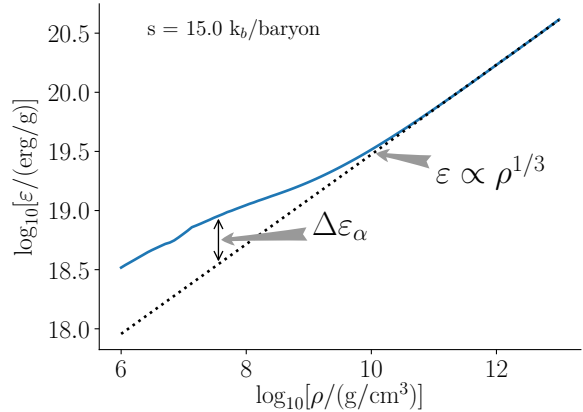


Figure 2. Specific internal energy (ϵ) vs. density ρ for an adiabat with $s = 15k_b$ /baryon. We use the tabulated EOS of Steiner et al. (2013). This figure illustrates the estimate for the heating by α recombination. For ρ around $10^{12} \text{ g cm}^{-3}$, the internal energy is dominated by photons and relativistic electrons and positrons. Hence, $\epsilon \propto \rho^{1/3}$. At lower densities, the free baryons start to combine to form α s. This raises the internal energy. The difference between the actual internal energy and the extrapolation is a good estimate for the energy added by α recombination.

shell, we average equations (1)-(3) over volume, using the Polytropic EoS, and the assumption that the mass flow through the gain region is negligible at the initiation of explosion:

$$\frac{dv}{dt} = -\frac{GM_{NS}}{r^2} + \frac{4\pi r^2 p}{M_g}, \quad (4)$$

$$\frac{dp}{dt} = -3\gamma \frac{pv}{r} + \frac{L_\nu \kappa (\gamma - 1)}{\frac{16}{3} \pi^2 r^5} M_g + \frac{3M_g}{4\pi r^3} (\gamma - 1) q_\alpha, \quad (5)$$

In these equations, v , p , and r represent average velocity, pressure, and radius for the shell. The last term in equation (5) vanishes for hypothesis II.

Again, for the initial conditions, we assume that the shell starts in hydrostatic equilibrium. However, at the moment that the evolution starts, there is no longer balance between the pressure gradient and gravity. Therefore, at $t=0$, we have the following initial conditions: $v = 0$, $r = r_0$ and $p = p_0 = \frac{GM_{NS}M_g}{4\pi r_0^4}$. To derive this latter condition, assume $dv/dt = 0$ in eq. (4).

To determine internal energy change due to α recombination (q_α), we note that the nuclear reaction rates are faster than the hydrodynamic rates. Therefore, the α fraction is in nuclear statistical equilibrium and is included in tabulated equations of state. At sufficiently high densities and/or temperatures, the α fraction is zero. Once material is heated to sufficiently high entropies, the material becomes unbound and expands away from the NS adiabatically. Figure 2 shows an adiabat with $s = 15 k_b$ /baryon from the tabulated EOS of Steiner et al. (2013). Following this adiabat down in density, the baryons recombine to form α s. In the process, the recombination releases energy raising the internal energy. We will use this to estimate the amount of energy liberated as a function of density.

The first step is to estimate the extra amount of internal energy due to the α recombination, $\Delta\varepsilon_\alpha$. For the region above the NS and below the shock, the EOS is dominated by relativistic electrons and positrons, photons, free nucleons, and α s. The partial pressure of the free nucleons and α s is described by a non-relativistic ideal gas. The electrons, positrons, and photons, which dominate the EOS are described by a degenerate and relativistic EOS. As a result, $\gamma \approx 4/3$. Under this approximation, $\varepsilon \propto \rho^{1/3}$. The dotted line in Figure 2 is a fit at the highest densities, the power-law index of this fit is 0.38. This is as expected given that the EOS is dominated by the relativistic species but also has some contribution from the nonrelativistic species. Extrapolating this fit to lower densities and comparing to the actual internal energy gives an estimate for how much internal energy is added due to α recombination, $\Delta\varepsilon_\alpha$.

The difference in the actual internal energy and the extrapolated roughly exhibits the following form

$$\Delta\varepsilon_\alpha = a \tanh\left(\frac{11 - \log_{10}\rho}{b}\right), \quad (6)$$

where $a = 6.67 \times 10^{18} \text{ erg/g}$ and $b = 2.147$ are the fitting parameters for the $s = 20 \text{ k}_b/\text{baryon}$ adiabat. We checked several other adiabats ($s = 5, 10, 15, 20 \text{ k}_b/\text{baryon}$) and found similar parameters. The heating rate due to α recombination, q_α is $\frac{3a}{b \ln(10)} \frac{v}{r} \cosh^{-2}\left(\frac{11 - \log_{10}\rho}{b}\right)$.

Defining the dimensionless parameters helps to illuminate the important physics and scalings. The dimensionless parameters of this model are as follows. We scale the radial coordinate by the initial position of the shell,

$$\tilde{r} = \frac{r}{r_0}, \quad (7)$$

the velocity by the dynamical velocity at r_0 ,

$$\tilde{v} = \frac{v}{v_0} = v \left(\frac{GM_{NS}}{r_0}\right)^{-1/2}, \quad (8)$$

the time coordinate by the dynamical time,

$$\tilde{t} = \frac{t}{t_0} = \frac{v_0}{r_0} t, \quad (9)$$

and the pressure by the initial hydrostatic pressure,

$$\tilde{p} = \frac{p}{p_0}. \quad (10)$$

The resulting dimensionless coupled set of ordinary differential equations are:

$$\frac{d\tilde{r}}{d\tilde{t}} = \tilde{v} \quad (11)$$

$$\frac{d\tilde{v}}{d\tilde{t}} = -\frac{1}{\tilde{r}^2} + \tilde{p}\tilde{r}^2, \quad (12)$$

$$\frac{d\tilde{p}}{d\tilde{t}} = -3\gamma \frac{\tilde{p}\tilde{v}}{\tilde{r}} + \frac{\eta}{\tilde{r}^5} + \frac{9(\gamma-1)}{b \ln(10)} \beta \frac{\tilde{v}}{\tilde{r}^4} \cosh^{-2}\left(\frac{11 - \log_{10}(\rho_0/\tilde{r}^3)}{b}\right), \quad (13)$$

where $\rho_0 = \frac{3M_g/4\pi r_0^3}{1\text{g/cm}^3}$ is the initial density of the system.

Other than the dimensionless variables, these equations depend upon three dimensionless parameters. One is γ ,

the adiabatic index for the EOS. The gain region is dominated by free nucleons, photon, and relativistic electrons and positrons. Therefore, for the rest of this manuscript, we consider γ to be fixed at a value a little above $4/3$. The second dimensionless parameter is

$$\eta = \frac{t_0}{t_H} = \frac{3L_\nu \kappa(\gamma-1)}{4\pi GM_{NS} v_0}, \quad (14)$$

which describes the ratio of dynamical time to heating time. The third dimensionless parameter is

$$\beta = \frac{a}{GM_{NS}/r_0} \quad (15)$$

which represents the maximum dimensionless internal energy change due to α recombination. For hypothesis II, explosion is dominated by neutrino heating, and $\beta = 0$.

In either case, the total dimensionless energy of the shell is:

$$\tilde{E}(\tilde{t}, \eta, \beta) = -\frac{1}{\tilde{r}} + \frac{\tilde{v}^2}{2} + \frac{\tilde{p}\tilde{r}^3}{3(\gamma-1)}. \quad (16)$$

This represents the explosion energy in this simple one-zone model. We also explicitly show that this dimensionless energy depends upon the dimensionless time, \tilde{t} , the heating parameter, η , and the recombination parameter β . In section 2.3, we show that η determines the final dimensionless explosion energy for hypothesis II, and both η and β determine the final dimensionless explosion energy for hypothesis I.

The dimensionful explosion energy in either case is

$$E = M_g v_0^2 \tilde{E}(\tilde{t}, \eta, \beta). \quad (17)$$

2.2 Perturbative Analysis

Before we present solutions to equations (11)-(13), we check the consistency of our model and equations with a perturbative analysis. In the previous section, we made several major assumptions that could affect the consistency of the equations. In particular, the one-zone assumption requires choices for divergences and variables that can affect the qualitative character of the evolution. One important constraint is that when there is neither external heating, $\eta = 0$, nor recombination, $\beta = 0$, then the zone should remain in hydrostatic balance. In other words, $dr/dt = 0$. If the position is perturbed, then it should oscillate about the hydrostatic position. Therefore, we perturb the equations with $\eta = 0$ and $\beta = 0$ to ensure that the solutions are stable.

The decomposed variables are $v = v'$, $r = r_0 + r'$, and $p = p_0 + p'$, and the resulting perturbed evolution equations are

$$\frac{d^2 r'}{dt^2} = \frac{4GM_{NS}}{r_0^3} r' + \frac{4\pi r_0^2}{M_g} p', \quad (18)$$

and

$$\frac{dp'}{dt} = -3\gamma \frac{p_0}{r_0} \frac{dr'}{dt}. \quad (19)$$

One may combine these equations into one second-order equation for v' . The solution of this second-order equation

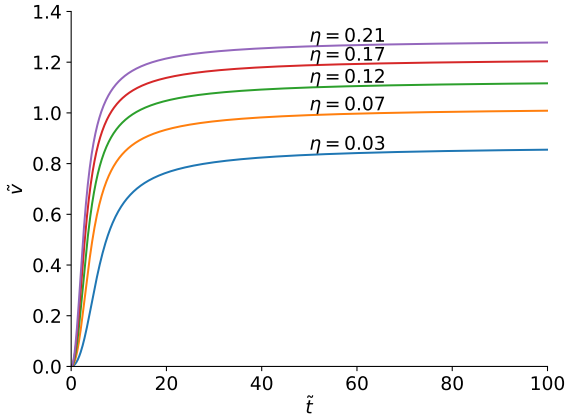


Figure 3. Solutions for the dimensionless velocity \bar{v} as a function of dimensionless time (\tilde{t}) and heating parameter (η) for hypothesis I. The other parameters are fixed at $r_0 = 150\text{km}$ and $M_g = 0.05 M_\odot$. The rise time of \bar{v} is mostly set by the dynamical timescale, while the value of velocity after infinite time is mostly set by η and β .

for v' is proportional to $e^{i\omega t}$. The resulting expression for the frequency is

$$\omega^2 = (3\gamma - 4) \frac{GM_{NS}}{r_0^3}. \quad (20)$$

As expected, solutions with $\gamma > 4/3$ oscillate about a hydrostatic equilibrium, and solutions with $\gamma < 4/3$ correspond to either exponentially decaying or expanding solutions. Therefore, despite the large assumptions, the model at least produces the correct linear behavior.

2.3 Solutions for Explosion Energy and Important Scalings

To solve the system of coupled differential equations (11)-(13), we use ODEINT from the `scipy.integrate` package. (ODEINT solves differential equations using LSODA from the FORTRAN library `odepack`.)

Figures 3 & 4 show the solutions for \bar{v} and \bar{p} as a function of time and the heating parameter, η for hypothesis I and for fixed values of $r_0 = 150\text{km}$ and $M_g = 0.05M_\odot$. The dynamical timescale, t_0 , sets the rise time for \bar{v} . The heating parameter mostly sets the asymptotic value of \bar{v} . Neutrino heating dominates the earliest phase until $\tilde{t} \approx 2$; neutrino heating falls off quite rapidly with radius, and as the gain region expands, it quickly leaves the source of neutrino heating. Instead, as the gain layer expands, adiabatic cooling dominates.

Figure 5, represents the solutions for explosion energy in the case of hypothesis I. In this case, the dimensionless explosion energy depends on three parameters: dimensionless time, heating parameter η , and β . As in hypothesis I, the explosion timescale is mostly determined by the dynamical timescale. For a fixed β , the explosion energy is set by η . It may appear that including β in the dynamics adds another parameter, increasing the number of independent parameters to 4. However, the dimensionful variables in β are

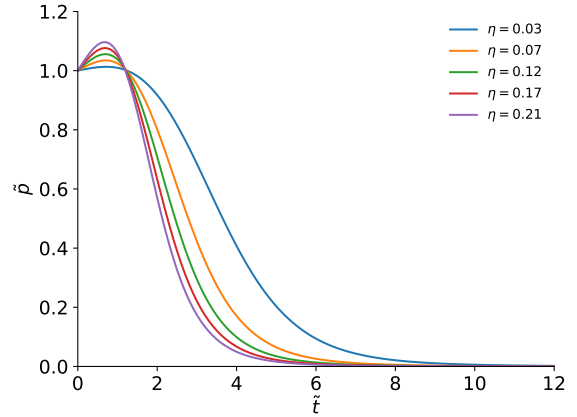


Figure 4. Solutions for the dimensionless pressure \bar{p} as a function of dimensionless time and \tilde{t} and heating parameter, η , for hypothesis I. The other parameters are fixed at $r_0 = 150\text{km}$ and $M_g = 0.05 M_\odot$. Until $\tilde{t} \approx 2$, neutrino heating dominates and pressure increases. Afterwards, adiabatic cooling dominates and pressure decreases. The maximum value of pressure is set by the heating parameter η .

already in the other dimensionless parameters. Therefore, there are still only three independent parameters.

Figure 6 shows the resulting solutions for dimensionless energy \tilde{E} as a function of \tilde{t} and η for hypothesis II. The value of \tilde{E}_∞ mostly depends on η , and the rise time mostly depends on the dynamical timescale, t_0 .

The explosion energy evolution depends upon three parameters. Equation (17) expresses the explosion energy in terms of mass in the gain region, M_g , the dynamical velocity, v_0 , and the dimensionless energy, \tilde{E} . In turn, \tilde{E} depends upon the dynamical timescale, t_0 , and the heating parameter, η . Upon first glance, it may appear that the explosion energy evolution depends upon four parameters. However, v_0 and t_0 are not independent; t_0 is proportional to r_0/v_0 . Furthermore, both v_0 and η depend upon the neutron star mass, M_{NS} .

In summary, there are three independent parameters that determine the explosion energy evolution. In section 3, we fit the explosion energy evolution of multi-dimensional simulations with our model. To do so, we may choose three parameters that are not entirely degenerate; we fit for the gain mass, M_g , the starting shock radius, r_0 , and the heating parameter, η .

2.4 Analytic and Asymptotic Behavior of Explosion Energy

In this section, we derive analytic solutions for the explosion energy for hypothesis I, including the asymptotic explosion energy, E_∞ . The evolution equation for the total dimensionless energy is

$$\frac{d\tilde{E}}{d\tilde{t}} = \frac{\eta}{3(\gamma - 1)\tilde{r}^2} + \frac{3\beta}{b \ln(10)} \frac{\bar{v}}{\tilde{r}} \cosh^{-2} \left(\frac{11 - \log_{10}(\rho_0/\tilde{r}^3)}{b} \right). \quad (21)$$

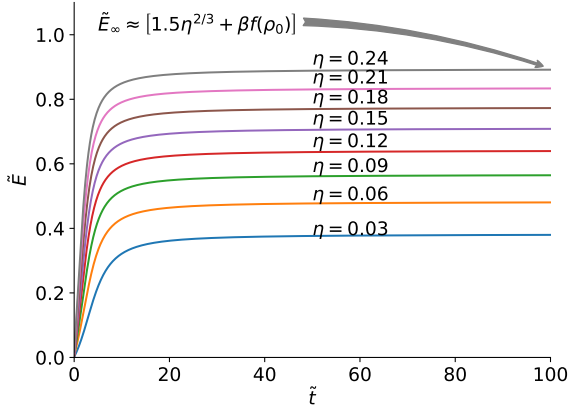


Figure 5. Dimensionless explosion energy $\tilde{E}(\tilde{t}, \eta, \beta)$ as a function of dimensionless time and heating parameter η for hypothesis I, for the fixed value of initial shock radius $r_0 = 150\text{km}$ (i.e. β). If $M_g = 0.05 M_\odot$, $M_{NS} = 1.4 M_\odot$, $r_0 = 150\text{ km}$ and $\kappa = 2 \times 10^{-17} \text{ cm}^2 \text{ g}^{-1}$, then $\eta = 0.12$ corresponds to a neutrino luminosity of $4.83 \times 10^{52} \frac{\text{erg}}{\text{s}}$. For most cases, the energy rises to 75% of \tilde{E}_∞ within $\tilde{t} = 3.5$. This rise time is set by the dynamical time; the asymptotic explosion energy is set by η and β ; see eq. (26).

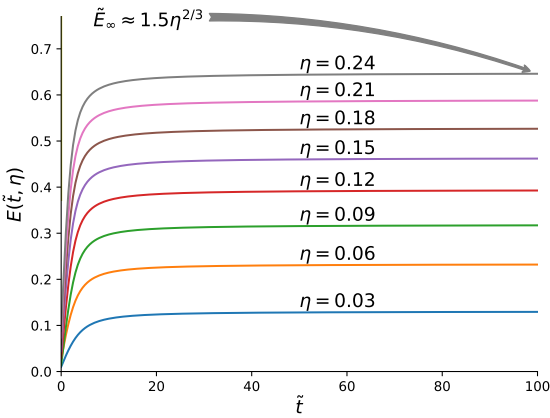


Figure 6. Similar to Figure 5 except for hypothesis II. As in hypothesis I, the rise time is mostly determined by the dynamical time. Since recombination offsets the dissociation during collapse for hypothesis II, the asymptotic energy is set by neutrinos (η) alone.

η and β are the constants of the model, so the path to analytic solution for \tilde{E} is to find a simple analytic solution for \tilde{r} . Since, $\tilde{v} = d\tilde{r}/dt$, our first challenge is to find an analytic solution for \tilde{v} . To do this, we consider a Taylor series expansion about $\tilde{t} = 0$. The initial conditions of this one-zone model gives the first two terms: $\tilde{v}(\tilde{t} = 0) = 0$ and $d\tilde{v}/d\tilde{t}(\tilde{t} = 0) = 0$. The leading order term is the second derivative with respect to \tilde{t} ; taking the time derivative of equation (12) gives

$$\frac{d^2\tilde{v}}{d\tilde{t}^2} = \frac{2\tilde{v}}{\tilde{r}^3} + 2\tilde{r}\tilde{v}\tilde{p} + \tilde{r}^2\frac{d\tilde{p}}{d\tilde{t}} = \eta. \quad (22)$$

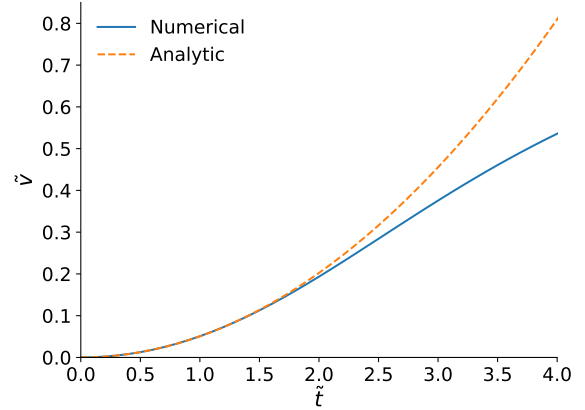


Figure 7. Dimensionless velocity \tilde{v} as a function of dimensionless time \tilde{t} for $\eta = 0.1$ and for hypothesis I. The solid line represents the numerical solution for velocity while the dashed line represents the quadratic approximation that we derive in equation (23). For small values of \tilde{t} , the numerical and analytic expressions match.

The third order derivative is zero.

Up to leading order, the dimensionless velocity evolution is

$$\tilde{v} = \frac{\eta}{2}\tilde{t}^2, \quad (23)$$

the evolution of the radius is

$$\tilde{r} = 1 + \frac{\eta\tilde{t}^3}{6}. \quad (24)$$

Substituting this analytic expression for \tilde{r} into equation (21) and integrating over all time leads to an estimate for the asymptotic explosion energy:

$$\begin{aligned} \tilde{E}_\infty = & \frac{6^{1/3}\eta^{2/3}}{3(\gamma-1)} \int_0^\infty \frac{d\tilde{t}'}{(1+\tilde{t}'^3)^2} \\ & + \frac{9\beta}{b \ln(10)} \int_0^\infty \frac{\tilde{t}'^2 d\tilde{t}'}{(1+\tilde{t}'^3)} \cosh^{-2}\left(\frac{11 - \log_{10}(\rho_0/(1+\tilde{t}'^3)^3)}{b}\right), \end{aligned} \quad (25)$$

where $\tilde{t}' = (\frac{\eta}{6})^{1/3}\tilde{t}$. Integrating leads to a simple analytic expression for the asymptotic explosion energy:

$$\tilde{E}_\infty \approx 1.5\eta^{2/3} + \beta \left(1 - \tanh\left(\frac{11 - \log_{10}(\rho_0)}{b}\right)\right). \quad (26)$$

Figures 7-9 compare these analytic solutions with the numerical solution of equations (12)- (13). First, Figure 7 compares the analytic solution for \tilde{v} with the numerical solution. As derived, the leading order is the second order term, and the value of the derivative is the heating parameter, η . For times later than $\tilde{t} \approx 2$, the analytic and numerical solutions begin to diverge. However, because \tilde{r}^2 appears in the denominator of the evolution equation for \tilde{E} , equation (21), the evolution of \tilde{E} is most sensitive to the early time evolution of \tilde{v} and \tilde{r} . Hence, the divergence between the analytic and numerical solutions at late times do not present a problem.

Figure 8 compares the analytic pressure with the numerical solution. To find the analytic pressure, we take the first derivative of the analytic velocity and use equation (12) to find a solution for \tilde{p} . In an absolute sense, the analytic

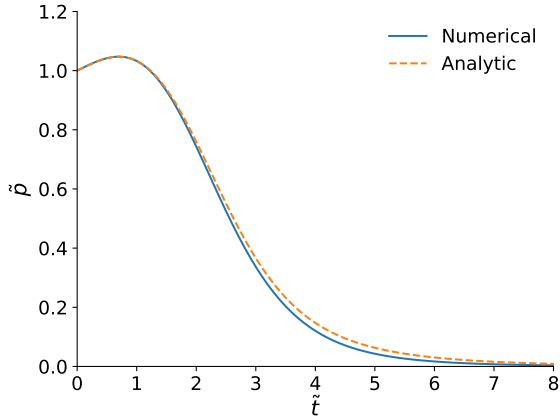


Figure 8. Dimensionless pressure \bar{p} as a function of dimensionless time \tilde{t} for $\eta = 0.1$ and for hypothesis I. As in Figure 7, the solid line represents the numerical solution for velocity, while the dashed line is the analytic solution of equation (12). The analytic approximations produce excellent agreement even at late times.

and numerical pressures agree for all time. This agreement is due to the radius appearing in the denominator of the integrand in equation (12). In a relative sense, the analytic and numerical solutions do diverge at late times in a similar way as for the velocity.

Figure 9 compares the analytic and numerical solutions for the asymptotic explosion energy as a function of η . The analytic result that $\tilde{E}_\infty \approx 1.5\eta^{2/3} + \beta \left(1 - \tanh\left(\frac{11 - \log_{10}(\rho_0)}{b}\right)\right)$ matches the numerical explosion within an accuracy of 15%.

In summary, the dimensional explosion energy for hypothesis I is $\tilde{E}_\infty \approx 1.5\eta^{2/3} + \beta \left(1 - \tanh\left(\frac{11 - \log_{10}(\rho_0)}{b}\right)\right)$ and for hypothesis II is $\tilde{E}_\infty \approx 1.5\eta^{2/3}$. The total explosion energy is

$$E_\infty \approx M_g v_0^2 \left[1.5\eta^{2/3} + \beta \left(1 - \tanh\left(\frac{11 - \log_{10}(\rho_0)}{b}\right)\right) \right]. \quad (27)$$

We find that for reasonable values of η , the recombination energy contributes a significant fraction of the explosion energy. For example, for $\eta = 0.15$, $M_g = 0.05M_\odot$, and $r_0 = 150\text{km}$, $\approx 50\%$ of the explosion energy is determined by α recombination.

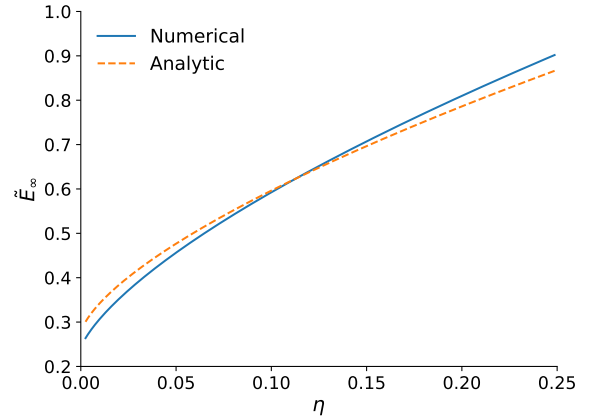


Figure 9. \tilde{E}_∞ as a function of η for hypothesis I. As in Figures 7 & 8, the solid line represents the numerical result, and the dashed line represents our analytic result, equation 26. We find that the analytic expression matches with numerical result with less than a 15% discrepancy.

3 COMPARING ANALYTIC THEORY WITH MULTI-DIMENSIONAL SIMULATIONS

As a preliminary test of the simple explosion model, we use Bayesian statistical inference to fit the model to multi-dimensional simulations. The simulations originate from four codes (CHIMERA, CoCoNuT-FMT, FORNAX2D, FORNAX3D), and a description of all four codes and their capabilities is summarized in Murphy et al. (2019). In essence, the explosion model is a theoretical prediction and we use the multi-dimensional simulations to test this prediction. The model has a characteristic curve defined by three parameters. This characteristic curve may or may not fit the explosion energy curves of the multi-dimensional simulations. If they do not fit, then this test would rule out the simple model. Even if the curve does fit, the model parameters may not match typical scenarios of core-collapse simulations. Our goal is to test the predictions of the simple model in two ways. For one, we will test if the model provides a good fit to the simulations. Second, if the model produces a good fit, we will assess whether the model parameters are reasonable.

With these two tests, broadly, there are three possible outcomes. For one, the model may produce a reasonable fit and parameters. This scenario would suggest that the model is a good theoretical description of the explosion evolution. Since the simple model is inherently spherical, we expect that explosions of low mass progenitors are the most likely to be consistent with the model. On the other hand, more massive progenitors tend to explode aspherically, so we do not expect the simple model to fit these inherently multi-dimensional explosions.

A second scenario is that the simple model fits the multi-dimensional results but the model parameters do not match typical simulation conditions. This would not completely rule out the model, but it would certainly call into question the fidelity of the model in representing the simulations.

The third scenario is that the model neither produces a reasonable fit nor reasonable parameters. This would rule

out the simple model as a good theory. The obviously multi-dimensional explosions of the most massive stars would likely fall into this category. This would also suggest (but not prove) that the development of the explosion dynamics are indeed multi-dimensional.

3.1 Bayesian Fitting

We use Bayesian statistical inference to both provide model fits and to infer the model parameters. Generically, Bayesian inference provides a way to statistically infer theory parameters given data. In this paper, the simple explosion model represents the theory, and the explosion energy evolution of the multi-dimensional simulation represents the data. The model parameters are $\theta = \{M_g, r_0, \eta\}$, and y is the explosion energy as a function of time for a single simulation.

The posterior distribution of the model parameters, θ given simulation explosion energy evolution, y is

$$p(\theta|y) = \frac{p(\theta)\mathcal{L}(y|\theta)}{p(y)}. \quad (28)$$

$p(\theta)$ is the prior distribution for the model parameters; for this initial analysis we assume uninformative (uniform) priors for all parameters. $\mathcal{L}(y|\theta)$ is the likelihood or sampling distribution, $p(y) = \sum_{\theta} p(\theta)p(y|\theta)$ is the normalization.

To construct the likelihood, we first consider the likelihood at each time, indexed by k :

$$\mathcal{L}_k(y|\theta) = \frac{1}{\sqrt{2\pi\epsilon^2}} e^{-\frac{(E_{\text{sim},k} - E_k)^2}{2\epsilon^2}}. \quad (29)$$

$E_{\text{sim},k}$ is the explosion energy at time index k , and E_k is the simple model explosion energy at the same time. ϵ represents scatter in the simulation, which might be due to inherent scatter in the underlying simulation or measurement of the explosion energy. In either case, this scatter is unknown and is a nuisance parameter. The total likelihood is

$$\mathcal{L}(y|\theta) = \prod_k \mathcal{L}_k(y|\theta). \quad (30)$$

To infer the posterior distribution, we use a Markov Chain Monte Carlo (MCMC) package called EMCEE (Foreman-Mackey et al. (2013), Goodman & Weare (2010)). EMCEE constructs posterior distribution by finding Likelihood function on each step of the calculation. This process requires information about explosion energy as a function of our set of parameters θ and is time-sensitive. We avoid solving our differential equations for each step in the chain by providing dimensionless energy $\tilde{E}(\tilde{t}, \eta, \beta)$ as a look-up table. Afterward, we interpolate the look-up table by using tri-linear interpolation. Again, our independent parameters are M_g, r_0 and η . To restrict the parameters to physically valid values, we set the bounds of the uniform priors to be $M_g < 0.5M_{\odot}$ and $\eta < 0.25$ (corresponding to neutrino luminosity $L < 10^{53} \text{ erg/s}$). For the MCMC runs, we typically use 100 walkers, 4000 steps and we burn 1000 of those.

3.1.1 Bayesian Fitting Results

Using Bayesian inference, we fit our theoretical model to multi-dimensional simulations. As expected, the theory fits those simulations that have mostly spherically symmetric

explosions and does not fit the predominantly aspherical explosions.

Figure 10 shows the Bayesian fits for hypothesis I (neutrino power + α recombination). The upper panel represents a sample of the good fits, and the lower panel shows some of the poor fits. Generally, the simulations in the top panel explode spherically and simulate the explosion of lower mass progenitors, while simulations in the lower panel explode aspherically and represent more massive progenitors. The explosion model is consistent with the spherical explosions, but is inconsistent with the aspherical explosions. This suggests that aspherical dynamics may be important in the explosion evolution of the aspherical explosions.

Figure 11 shows the posterior distributions for the good fits (top panel of Figure 10). The best-fit model parameters for each simulation are as follows: FORNAX2D n8.8 — $M_g = 0.0413^{+0.0032}_{-0.0027} M_{\odot}$, $r_0 = 411^{+60}_{-68} \text{ km}$, $\eta = 0.07^{+0.02}_{-0.04}$; FORNAX2D u8.1 — $M_g = 0.0353^{+0.0029}_{-0.0021} M_{\odot}$, $r_0 = 567^{+74}_{-93} \text{ km}$, $\eta = 0.06^{+0.02}_{-0.03}$; FORNAX2D z9.6 — $M_g = 0.0326^{+0.0020}_{-0.0015} M_{\odot}$, $r_0 = 465^{+46}_{-59} \text{ km}$, $\eta = 0.07^{+0.01}_{-0.02}$; CHIMERA 12 — $M_g = 0.1039^{+0.0052}_{-0.0046} M_{\odot}$, $r_0 = 690^{+59}_{-66} \text{ km}$, $\eta = 0.07^{+0.01}_{-0.01}$; CoCoNuT-FMT z9.6 — $M_g = 0.0432^{+0.0012}_{-0.0012} M_{\odot}$, $r_0 = 407^{+11}_{-11} \text{ km}$, $\eta = 0.04^{+0.00}_{-0.00}$. The uncertainties represent the 68% highest density confidence intervals. In addition to providing a good fit, these parameters are also roughly consistent with values measured in CCSN simulations. A detailed comparison with the simulations could help to further constrain the theoretical model.

Figure 12 shows the Bayesian fits for hypothesis II (neutrino power only). As in Figure 10, the upper panel presents good fits, while the lower panel shows some of the poor fits. Again, the simulations on the top panel explode spherically, while those in the lower panel explode aspherically. The fact that our spherically symmetric model fits the simulations given on the top panel and cannot fit lower ones is consistent with the hypothesis that some simulations explode spherically while others are dominated by aspherical dynamics.

3.2 Goodness-of-fit with Predictive Posterior Checking

An MCMC method will find the most likely model parameters, but it does not determine whether the theory and model are a good fit to the simulation data. Therefore, we use posterior predictive checking to check for goodness-of-fit. The goal of this technique is to compare the predicted “data” from the simple model with the “data” from the simulations. If the model produces a good fit, then the predicted “data” should match the simulation “data”.

As before, y represents the “data” or explosion energy as a function of time from the simulations. y^{rep} represents the replicated “data” from the model, and θ are the model parameters. In the previous section, we describe how to infer the model parameters, θ , given the data, y . One then may use those model parameters to calculate the model explosion energy curve; this is the replicated data, y^{rep} , given the original data, y , or explosion energy curve from the simulation. The goal of our goodness-of-fit test is to compare the replicated data with the original data.

The following describes the specific goodness-of-fit test

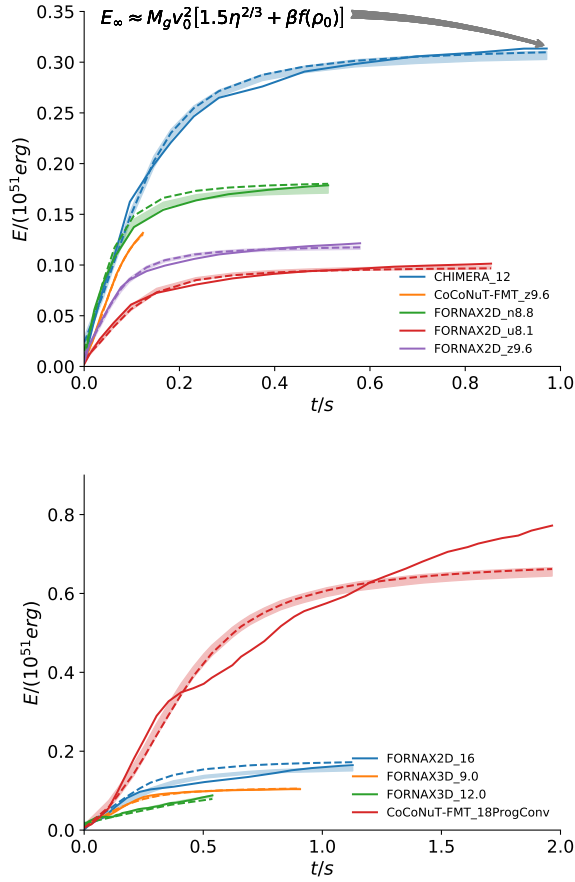


Figure 10. Explosion energy vs time after bounce for hypothesis I (neutrino power + α recombination). The solid lines represent the simulation curves, while the shaded bands represent fits of the theoretical model. The dashed line represents energy curve for the best fit. The upper panel shows the five models with good fits and reasonable parameters; the bottom panel shows some of the poor fits. In general, the good fits represent simulations of low progenitor masses, which explode mostly spherically. The poor fits represent higher progenitor mass simulations, which tend to explode aspherically. The analytic explosion model is consistent with the mostly spherically symmetric explosion, and, not surprisingly, it is not consistent with the aspherical explosions. This suggests that aspherical dynamics are important in determining eventual explosion energies for the higher progenitor mass simulations.

that we use. First of all, note that there are N_s replicated data for each time, t_k , where N_s is the number of MCMC samples. If the replicated data is a good representation (i.e. good fit) of the data, then half of these replicated data should be above the data at time t_k and the other half should be below. This is the essence of our goodness-of-fit test. The first step is to calculate the probability that $y_k^{\text{rep}} \leq y_k$:

$$P_{\leq} = P_k \left(y_k^{\text{rep}} \leq y_k \right) = \int P(y_k^{\text{rep}} \leq y_k | \theta) P(\theta | y) d\theta. \quad (31)$$

In practice the right-hand is discrete. At each time t_k , we calculate replicated data by taking the N_s MCMC samples of θ as inputs to our model. This generates N_s replicated data at each time t_k . We then calculate the fraction of these

replicated data that are less than or equal to the data (explosion energy from simulation).

If the replicated data accurately represents the data, then P_{\leq} should be distributed as a uniform distribution between 0 and 1:

$$P(P_{\leq}) \sim \mathcal{U}(0, 1), \quad (32)$$

where $P(P_{\leq})$ is the distribution of P_{\leq} for all times, and $\mathcal{U}(0, 1)$ is the uniform distribution. To test whether $P(P_{\leq})$ is indeed drawn from the uniform distribution, we use the one-sided Kolmogorov-Smirnov test.

3.3 Goodness-of-fit Results

Figure 13 shows the goodness-of-fit probability, P_{\leq} , as a function of time for hypothesis I. Each set of dots represents the fit of one simulation. The top panel shows the fits which are consistent with a uniform distribution for P_{\leq} from 0 to 1. The fact that they do represent a normal distribution is a good indicator that the model does fit the simulation results. The bottom panel shows a few examples that are poor fits. For each of these poor fits, the average value of P_{\leq} is around 0.5. However, the distribution is not uniformly distributed from 0 to 1; the values tend to bunch up around 0 and 1, indicating that the model is often far from the simulation data.

Figure 14 shows the cumulative distribution of the goodness-of-fit probabilities for hypothesis I. Again, each cumulative distribution represents a fit to one simulation, the top panel shows fits which have a uniform distribution for P_{\leq} representing a good fit, and the bottom panel shows the simulations which exhibit a bad fit. In general, core-collapse simulations of more massive stars exhibit poor fits. This is consistent with the expectation that the explosion energy model of this manuscript is spherical in nature, the low mass explosions are mostly spherical, and the higher mass explosions are multi-dimensional.

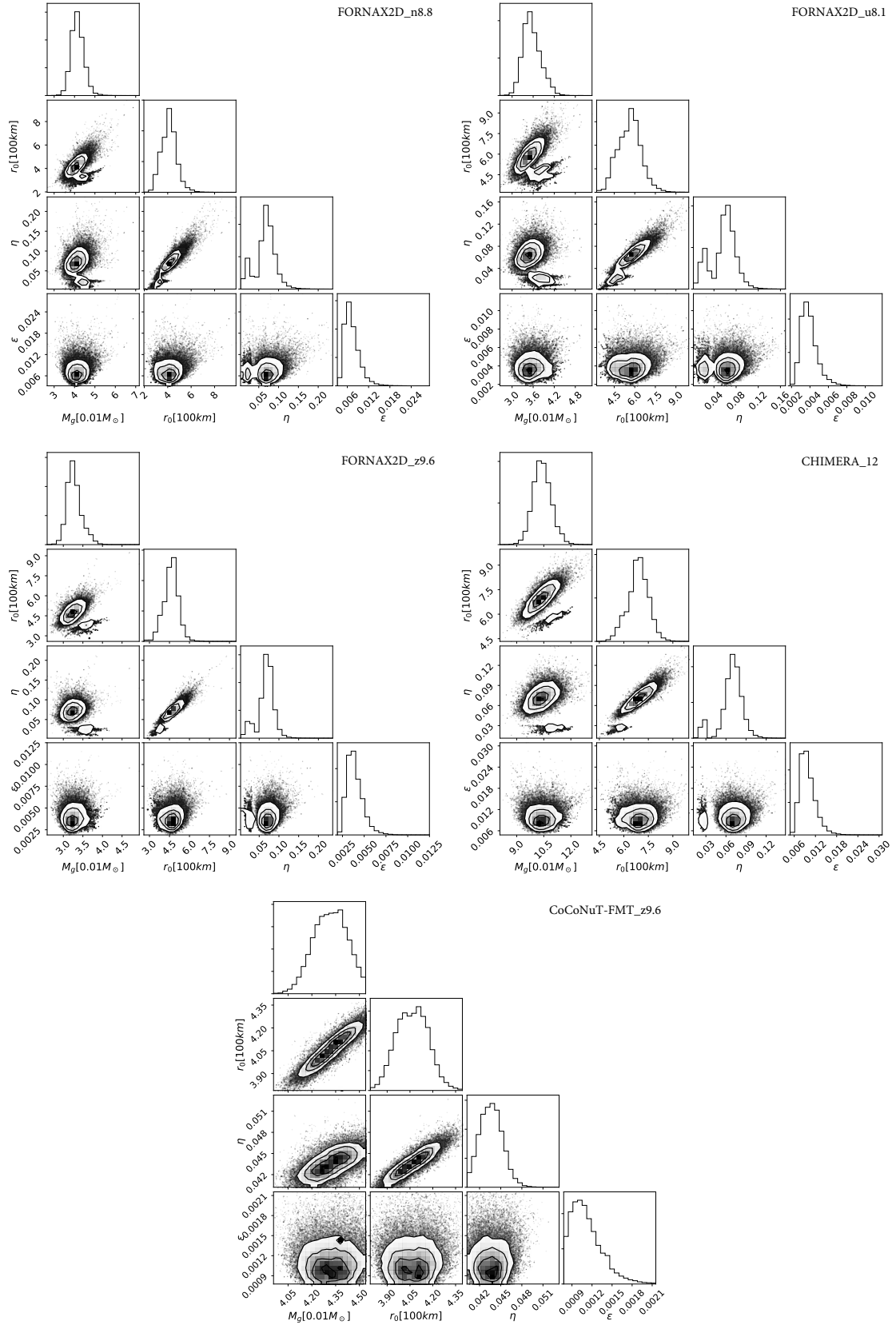


Figure 11. The posterior distribution for the explosion model parameters, M_g , r_0 , η , and ϵ for hypothesis I. This fit corresponds to Fornax2D n8.8 (Radice et al. 2017), Fornax2D u8.1 (Radice et al. 2017), Fornax2D z9.6 (Radice et al. 2017), Chimera 12 (Bruenn et al. 2016b), CoCoNuT-FMT z9.6 (Müller et al. 2019). There is a degeneracy among the parameters given by eq. (14).

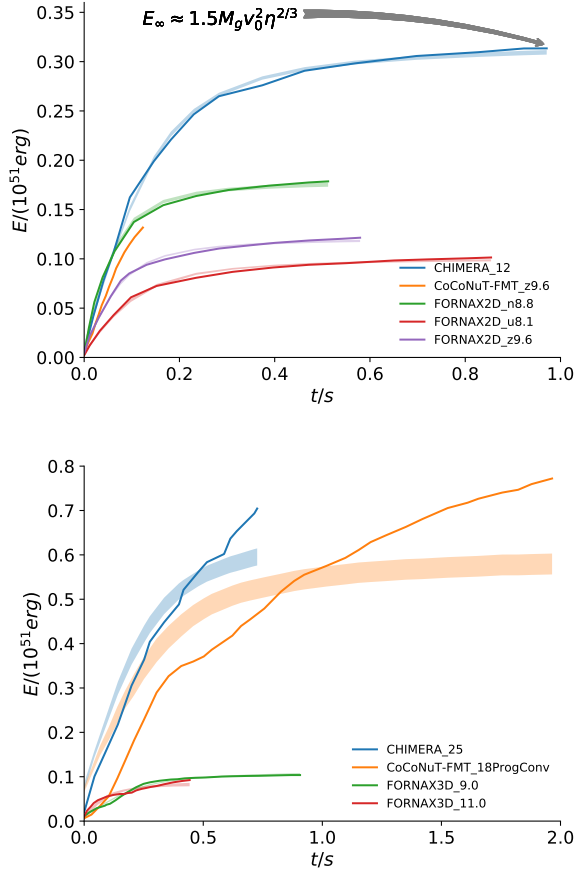


Figure 12. Similar to Figure 10 except for hypothesis II. As is the case for hypothesis I, the explosion model of hypothesis II is consistent with the mostly spherically symmetric explosion and not consistent with the aspherical explosions. Again, this suggests that aspherical dynamics are important in determining eventual explosion energies of the higher progenitor mass simulations.

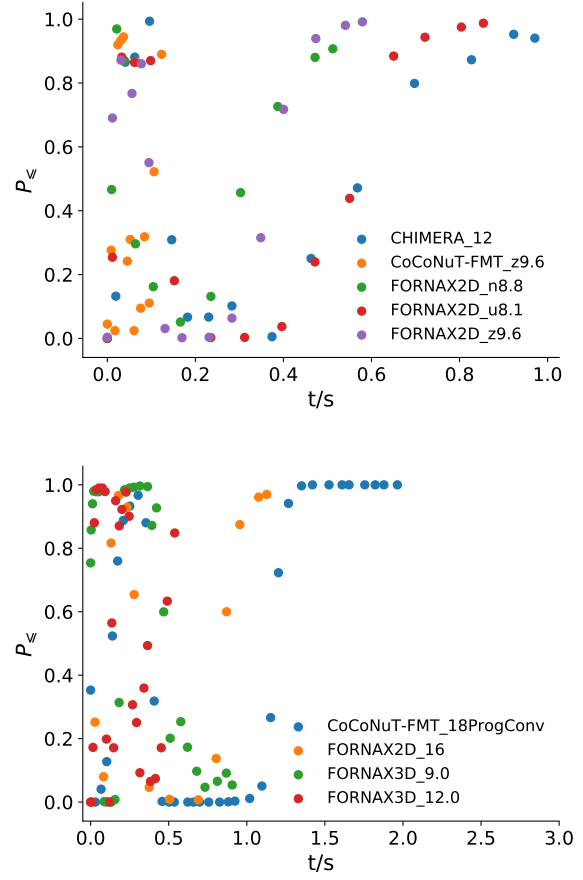


Figure 13. P-value vs time for hypothesis I. For a good fit, the p-value should be randomly distributed about from 0 to 1. The top panel shows good fits, and the bottom panel shows models with poor fits. Figures 14 & 15 show the corresponding cumulative distributions and KS tests.

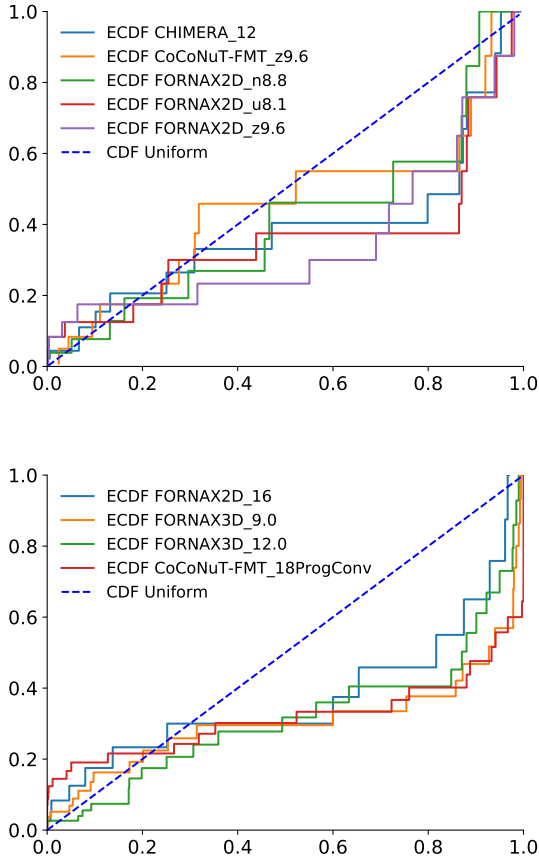


Figure 14. Cumulative distribution for good (upper panel) and poor (lower panel) fits for hypothesis I. The solid lines represent the P-value cumulative distributions for each simulation fit while the dashed line represents a uniform distribution. A good fit should have P-values that are uniformly distributed between 0 and 1. The fits in the top panel are consistent with a uniform distribution, and the fits in the bottom panel are inconsistent with a uniform distribution. As expected, the model is most consistent with simulations that explode spherically (top panel).

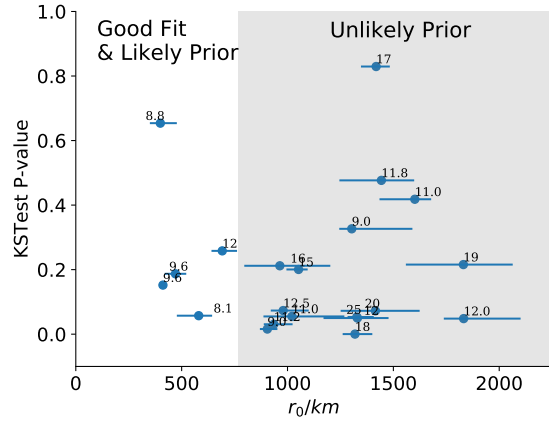


Figure 15. One-sided Kolmogorov-Smirnov test result- p-value vs the initial shock radius, r_0 for hypothesis I. Fits with high KS P-values are good fits by definition, but those with high r_0 likely do not represent the conditions of CCSN simulations. Therefore, we only consider those with large KS P-values and r_0 below 800 km both a good fit and a reasonable representation of the CCSN simulations. For the five simulations that satisfy these conditions, they show spherical explosions. As expected our explosion model provides reasonable fits for spherical explosions. The other fits that do not fit or have large r_0 show aspherical explosions.

4 DISCUSSION AND CONCLUSION

We present a spherically symmetric theoretical model for CCSN explosion energies. In this model, we make the following assumptions: 1) explosion is driven by the delayed-neutrino mechanism and α recombination may play an important role, 2) the neutrino luminosity is constant, 3) we follow the dynamic evolution of a spherically symmetric, one-zone gain region, 4) mass accretion is negligible, 5) the gain region starts in hydrostatic equilibrium. To include α recombination energy, we developed two hypotheses. I) The explosion energy is set by both neutrino power and α recombination; II) α recombination offsets α dissociation during collapse and the explosion energy is powered by neutrinos alone. Given these assumptions, we propose important scales for dimensional analysis, find solutions to the dimensionless evolution, and derive analytic scalings. We find that both hypotheses are consistent with the explosions of low mass progenitors which also exhibit mostly spherical explosions; both hypotheses are inconsistent with the explosion energies of the more massive progenitors, which also tend to explode aspherically. This inconsistency suggests that the explosion dynamics of high mass progenitors is in part determined by multi-dimensional dynamics. For the mostly spherical explosions, we find that the evolution of the dimensionless explosion energy, \tilde{E} depends upon two dimensionless parameters, η , and β in the case of hypothesis I and one dimensionless parameter η in the case of hypothesis II. Finally, we derive an analytic expression for the asymptotic explosion energy: $E_\infty \approx M_g v_0^2 \left[1.5\eta^{2/3} + \beta f(\rho_0) \right]$, where $\beta = 0$ in the case of hypothesis II (neutrino heating only).

A survey of the literature reveals three other semi-analytic or analytic investigations of explosion energy; however, those investigations had different goals and results. In particular, these previous investigations did not focus on deriving the analytic scalings nor did those investigators directly compare their predictions with multi-dimensional simulations.

The theoretical model in Janka (2001) considered a boundary value problem and assumed three regions (hydrostatic cooling, hydrostatic heating, and free-fall layers). While this model presented both an explosion condition and explosion energy evolution, there were many parameters in the model. As a result, it is not clear which parameters determine the explosion energy evolution. Also, this study did not compare the theoretical explosion evolution with multi-dimensional simulations.

Müller et al. (2016) presented a model that considers explosion as a two-phase process. The pre-explosion phase is described by the three-layer model of Janka (2001). The model for the explosion phase is similar to the one presented in this manuscript; it is a spherically-symmetric one-zone model. However, the primary goal of the Müller et al. (2016) explosion model is to infer explosion energies given a progenitor structure. The model does not give evolution of the explosion energy, nor does it represent the final explosion energy in terms of L_ν , M_{NS} , etc.

Moreover, Müller et al. (2016) scale the energy by the recombination energy of neutrons and protons into Fe rather than the gravitational energy of gain region. During collapse, the matter loses internal energy when the Fe disassociates to free neutrons and protons, and during explosion, mat-

ter regains that energy when the free baryons recombine into bound nuclei. Given these facts, one might expect the dissociation and recombination of Fe have no net effect on the explosion energy. Müller et al. (2016) suggest that the condition for explosion is met when neutrinos heat the gain region enough to offset the initial Fe dissociation. In this scenario, the explosion energy is set by Fe recombination and the amount of mass ejected. In this paper, we investigate the role of recombination in the explosion energy evolution. We discuss two hypotheses in which explosion energy is powered by I) neutrino heating+ α recombination and II) neutrino heating only. In difference of Müller et al. (2016) paper, in both our hypotheses neutrino heating directly contributes in the explosion energy. Both of the hypotheses fit low mass spherically symmetric explosions. We do not distinguish between the two. However, Müller et al. (2016) note a correlation between explosion energy and the Fe recombination for 2D simulations. This prior might suggest that hypothesis I is the theory explaining energy evolution of the spherically symmetric exolosions.

We recommend further numerical investigations into whether the explosion energy depends upon the recombination. Further detailed analyses of numerical simulations will undoubtedly help to resolve this mystery. Hypothesis I predicts $E_\infty/M_g v_0^2 \left[1.5\eta^{2/3} + \beta f(\rho_0) \right] \sim 1$, a prediction that is easily falsifiable by multidimensional simulations of low mass progenitors.

Papish et al. (2015) presented an order of magnitude analysis for the explosion energy. They found that the delayed-neutrino mechanism can not yield explosions with energies more than about $0.5 \times 10^{51} \text{erg}$. They then conclude that the neutrino mechanism is incapable of generating explosion energies that are inferred from observations. However, our analysis shows that an explosion model based upon the delayed neutrino mechanism is consistent with the least energetic, spherically symmetric explosions in multi-dimensional simulations. Including aspherical dynamics in the model could increase the explosion energy. Therefore, we find it premature to rule out the delayed neutrino mechanism.

Murphy et al. (2019) found that recent multi-dimensional simulations are under-energetic compared to the explosion energies inferred from observations by at least a factor of 2. The resolution in this discrepancy may result from either improved simulations or inferences of explosion energies from observations. With regard to the simulations, is it even possible for the explosions energies to increase by more than a factor of 2? One may use the analytic explosion energy equation (eq. (27)) to investigate the sensitivity of the simulated explosion energies. However, given that this model only explains the spherical explosions, a complete sensitivity study must await an explosion energy theory that includes multi-dimensional dynamics.

ACKNOWLEDGEMENTS

We thank Peter Höflich, Raphael Hix, and Frank Timmes for discussions concerning Fe and α recombination.

BIBLIOGRAPHY

- Benz W., Colgate S. A., Herant M., 1994, *Physica D: Nonlinear Phenomena*, 77, 305
- Bethe H. A., Wilson J. R., 1985, *ApJ*, 295, 14
- Bruenn S. W., Dirk C. J., Mezzacappa A., Hayes J. C., Blondin J. M., Hix W. R., Messer O. E. B., 2006, *Journal of Physics: Conference Series*, 46, 393
- Bruenn S. W., et al., 2016b, *ApJ*, 818, 123
- Bruenn S. W., et al., 2016a, *The Astrophysical Journal*, 818, 123
- Buras R., Rampp M., Janka H. T., Kifonidis K., 2003, *Phys. Rev. Lett.*, 90, 241101
- Buras R., Janka H. T., Rampp M., Kifonidis K., 2006, *A&A*, 457, 281
- Burrows A., Hayes J., Fryxell B. A., 1995, *ApJ*, 450, 830
- Colgate S. A., White R. H., 1966, *ApJ*, 143, 626
- Fernández R., Thompson C., 2009, *The Astrophysical Journal*, 703, 1464
- Foreman-Mackey D., Hogg D. W., Lang D., Goodman J., 2013, *Publications of the Astronomical Society of the Pacific*, 125, 306
- Goodman J., Weare J., 2010, *Commun. Appl. Math. Comput. Sci.*, 5, 65
- Herant M., Benz W., Hix W. R., Fryer C. L., Colgate S. A., 1994, *ApJ*, 435, 339
- Janka H. T., 2001, *A&A*, 368, 527
- Janka H. T., Mueller E., 1995, *ApJ*, 448, L109
- Kitaura F. S., Janka H. T., Hillebrandt W., 2006, *A&A*, 450, 345
- Lentz E. J., et al., 2015, *The Astrophysical Journal*, 807, L31
- Liebendörfer M., Mezzacappa A., Thielemann F.-K., 2001a, *Phys. Rev. D*, 63, 104003
- Liebendörfer M., Mezzacappa A., Thielemann F.-K., Messer O. E., Hix W. R., Bruenn S. W., 2001b, *Phys. Rev. D*, 63, 103004
- Liebendörfer M., Rampp M., Janka H. T., Mezzacappa A., 2005, *ApJ*, 620, 840
- Mabanta Q. A., Murphy J. W., 2018, *ApJ*, 856, 22
- Mac Low M.-M., Klessen R. S., 2004, *Rev. Mod. Phys.*, 76, 125
- Müller B., Heger A., Liptai D., Cameron J. B., 2016, *MNRAS*, 460, 742
- Müller B., Melson T., Heger A., Janka H.-T., 2017, *MNRAS*, 472, 491
- Murphy J. W., Burrows A., 2008, *ApJ*, 688, 1159
- Murphy J. W., Dolence J. C., 2017, *The Astrophysical Journal*, 834, 183
- Murphy J. W., Mabanta Q., Dolence J. C., 2019, *Monthly Notices of the Royal Astronomical Society*, 489, 641
- Müller B., 2015, *Monthly Notices of the Royal Astronomical Society*, 453, 287
- Müller B., et al., 2019, *Monthly Notices of the Royal Astronomical Society*, 484, 3307
- Papish O., Nordhaus J., Soker N., 2015, *Monthly Notices of the Royal Astronomical Society*, 448, 2362
- Radice D., Burrows A., Vartanyan D., Skinner M. A., Dolence J. C., 2017, *ApJ*, 850, 43
- Rampp M., Janka H. T., 2002, *A&A*, 396, 361
- Skinner M. A., Dolence J. C., Burrows A., Radice D., Vartanyan D., 2019, *ApJS*, 241, 7
- Steiner A. W., Hempel M., Fischer T., 2013, *The Astrophysical Journal*, 774, 17
- Thompson T. A., Burrows A., Pinto P. A., 2003, *ApJ*, 592, 434
- Vartanyan D., Burrows A., Radice D., Skinner M. A., Dolence J., 2018a, *Monthly Notices of the Royal Astronomical Society*, 482, 351
- Vartanyan D., Burrows A., Radice D., Skinner M. A., Dolence J., 2018b, *Monthly Notices of the Royal Astronomical Society*, 482, 351
- Woosley S. E., Heger A., Weaver T. A., 2002, *Reviews of Modern*

Physics, 74, 1015

This paper has been typeset from a $\text{\TeX}/\text{\LaTeX}$ file prepared by the author.